Low temperature performance of graphite and LiNi0.6Co0.2Mn0.2O2 electrodes in Li-ion batteries

ARTICLE *in* JOURNAL OF MATERIALS SCIENCE · NOVEMBER 2014

Impact Factor: 2.37 · DOI: 10.1007/s10853-014-8479-6

10 AUTHORS, INCLUDING:

Adnan Yaqub
Korea Electrotechnology Research Institute…
10 PUBLICATIONS **31** CITATIONS
SEE PROFILE

Atif Pervez
Korea Electrotechnology Research Institute…
15 PUBLICATIONS **31** CITATIONS
SEE PROFILE

Umer Farooq
Korea Electrotechnology Research Institute…
12 PUBLICATIONS **31** CITATIONS
SEE PROFILE

Haeyoung Choi
Korea Electrotechnology Research Institute…
24 PUBLICATIONS **104** CITATIONS
SEE PROFILE

Low temperature performance of graphite and $LiNi_{0.6}Co_{0.2}Mn_{0.2}O_2$ electrodes in Li-ion batteries

Adnan Yaqub, You-Jin Lee, Min Ji Hwang, Syed Atif Pervez, Umer Farooq, Jeong-Hee Choi, Doohun Kim, Hae-Young Choi, Seong-Back Cho, et

Journal of Materials Science
Full Set - Includes `Journal of Materials Science Letters'

ISSN 0022-2461

J Mater Sci
DOI 10.1007/s10853-014-8479-6

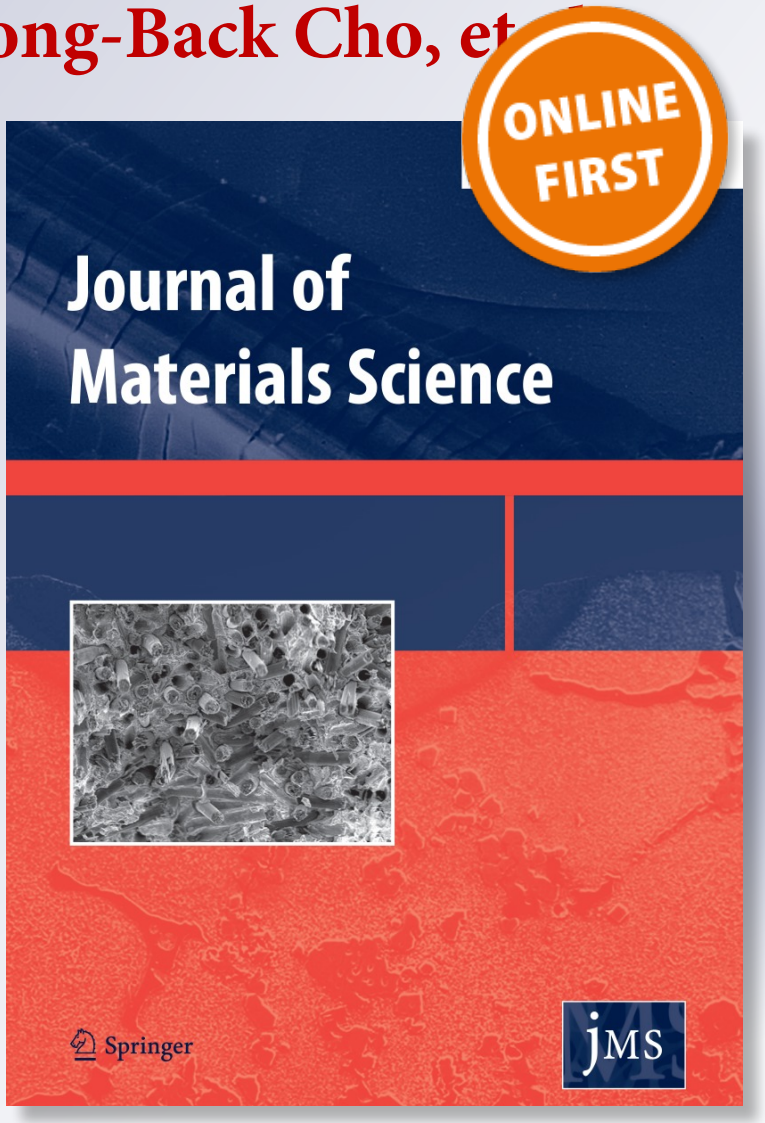

Springer

J Mater Sci
DOI 10.1007/s10853-014-8479-6

Low temperature performance of graphite and $LiNi_{0.6}Co_{0.2}Mn_{0.2}O_2$ electrodes in Li-ion batteries

Adnan Yaqub · You-Jin Lee · Min Ji Hwang · Syed Atif Pervez · Umer Farooq · Jeong-Hee Choi · Doohun Kim · Hae-Young Choi · Seong-Back Cho · Chil-Hoon Doh

Received: 22 April 2014 / Accepted: 15 July 2014

Abstract Low temperature (LT) behavior of graphite/$LiNi_{0.6}Co_{0.2}Mn_{0.2}O_2$ (NCM622) cells prepared with low loading or LL (thinner electrodes prepared with low loading and packing density) and high loading or HL (thicker electrodes prepared with high loading and packing density) were investigated. The cells were prepared as half coin cell, full coin cell, and full pouch cell to identify the main factors that limit LT operations of lithium ion batteries. All the cells were tested at −32 °C, and the capacity retention at LT was compared to the capacity retention at room temperature (RT). The Li^+ insertion kinetics was analyzed by electrochemical impedance spectroscopy. The LL electrodes showed a lesser charge transfer resistance (R_{ct}) than that shown by the thicker electrodes at LT. The diffusion coefficients of Li^+ calculated via the galvanostatic intermittent titration technique (GITT) in graphite and NCM622 electrodes prepared with LL and HL at RT were in the range of 10^{-8} cm^2/s but decreased to the range of 10^{-13} and 10^{-11} cm^2/s at −32 °C, respectively. GITT results confirmed that the capacity loss at LT, with increased electrode loading, arose from the limitation of Li-ion diffusion within the electrode.

A. Yaqub · Y.-J. Lee · M. J. Hwang · S. A. Pervez · U. Farooq · J.-H. Choi · D. Kim · H.-Y. Choi · C.-H. Doh (✉)
Battery Research Center, Korea Electro-Technology Research Institute (KERI), Changwon 642-120, Republic of Korea
e-mail: chdoh@keri.re.kr

A. Yaqub · S. A. Pervez · U. Farooq · C.-H. Doh
Department of Electrical Functionality Material Engineering, University of Science and Technology, Daejeon 305-333, Republic of Korea

S.-B. Cho
The 4th R&D/3, Agency for Defense Development, Daejeon 305-600, Republic of Korea

Introduction

Lithium-ion batteries (LIBs) have shown an ever-increasing demand as power sources for portable devices such as cellular phones, laptop computers, digital cameras, hybrid electric vehicles, and smart grid applications [1, 2]. In this context, common electrode materials such as Si [3], transition metal oxides [4, 5], graphite [6, 7], and NCM622 [8] are very popular in the LIB industry. In most cases, the room temperature behavior of these electrodes is generally reported but reports on their low temperature behavior are not so common. LIBs function appropriately at room temperature, but their poor electrochemical performance is one of the major technical barriers to greater efficiency as a power source at low temperature [9–12]. It has been reported that when the temperature falls below −20 °C, both the power and energy density of LIBs are significantly reduced [13–15].

To meet the high energy density, power, and improved cycling demands for batteries, most efforts have been directed toward fabricating, optimizing, and enhancing the performance of electrodes [16–20]. With respect to electrode design, electrode thickness, active material loading, electrode packing density, and chemical composition are the important parameters that affect the electrochemical performance of the cell. It is also believed that, morphology and structure of the electrodes have a great impact not only on the electrochemical properties of the cell but also on the lithium deposition on the surface of the electrodes. It has also been found that electrode loading has an extraordinary effect on the energy density of an electrode [21–26].

Although low-temperature performances of LIBs have been well studied, no investigations have been undertaken to-date to understand the effect of electrode loading (loading amount, packing density, and thickness) on the low

Published online: 02 August 2014

Table 1 Loading parameters; electrode loading amount, electrode thickness, and electrode packing density calculated for anode and cathode of half coin cell, full coin cell, and full pouch cell

LD type	Half coin cell						Full coin cell						Full pouch cell					
	Cathode			Anode			Cathode			Anode			Cathode			Anode		
	LD	Th	PD	LD	Th	PD	LD	Th	PD	LD	Th	PD	LD	Th	PD	LD	TH	PD
LL	6.4	53	1.20	3.83	54	0.71	6.3	52	1.21	3.9	53	0.75	6.6	53	1.24	4	54	0.74
HL	15.33	55	2.78	9.42	70	1.35	14.88	55	2.70	9.5	70	1.35	15.09	55	2.74	9.37	70	1.34

LD loading amount (mg/cm^2), *Th* thickness (μm), *PD* packing density (g/cc)

temperature performances of graphite and NCM622 electrodes. Therefore, a systematic study was initiated in our group to investigate the effect of electrode loading onto three cell assembly types (half coin cell, full coin cell, and full pouch cell), prepared with both low and high level loadings of the active material. All the cells were charged/discharged via CC-CV/CC methods both at room temperature (RT; 25 °C) and low temperature (LT; −32 °C). In this study, the galvanostatic intermittent titration technique (GITT) was used to determine the diffusion coefficient of lithium in the working electrode and electrochemical impedance spectroscopy (EIS) was adopted to study impedance of the half coin cells and also to evaluate its performance at LT.

Experimental

Pitch-coated natural graphite (99.95 %; BTR Energy Materials Co., Ltd., China) and $LiNi_{0.6}Co_{0.2}Mn_{0.2}O_2$ (NCM622; L&F Co., Ltd., Korea) were used as active materials for anode and cathode, respectively. The graphite and NCM622 samples used in this study had a mean particle size of 17.1 and 12.0 μm, and surface area of 2.11 and 0.22 $m^2\ g^{-1}$, respectively that were determined by Brunauer–Emmett–Teller (BET) method.

To obtain anode and cathode laminates with LL and HL, graphite/NCM622 slurries were prepared by mixing 90 % of the active material, 5 % PVDF (polyvinylidene fluoride) binder, and 5 % SPB (Super-P carbon black) conductive material in NMP (*N*-Methyl-2-pyrrolidone) solvent, according to the standard procedure. A mechanical mixing of the above components was carried out at 2000 rpm for 30 min. The slurry was then coated onto Cu foils (anode) and Al foils (cathode) by using a doctor blade. Different loadings in the anode and cathode electrodes were obtained by varying the height of the doctor blade. The loading parameters of the electrode loading amount (mg/cm^2), the electrode packing density (g/cc), and the electrode thickness (μm) for the LL and HL anode and cathode electrodes of the three cell assembly types are reported in Table 1.

Three types of cell assemblies were prepared by using LL and HL electrodes in a dry room. The separator employed was Celgard 2325. The electrolyte was a mixture of 1 M $LiPF_6$ dissolved in ethylene carbonate (EC)/ethyl methyl carbonate (EMC)/di-methyl carbonate (DMC) (1/1/1 by volume). The half-cells were assembled with the standard 2023 coin cell hardware (Wellcos Co. Korea). Lithium metal (purity 99.9 %, Hohsen Co. Japan) was used as a reference electrode against graphite anode and NCM622 cathode electrode. The cells were charged/discharged in a CC-CV/CC mode within a potential range of 0.005–1.5 V (anode) and 2.5–4.3 V (cathode). The full-cells (full coin cell and full pouch cell) consisted of graphite anode and NCM622 cathode, prepared with negative/positive (N/P) ratio ≥1.10 and charged/discharged in a CC-CV/CC mode within a potential range of 2.5–4.2 V.

All types of the cells were pre-cycled with a minimum current of 0.1 C for 2 cycles. Later, the cells were charged and discharged sequentially at RT (3–7 cycles), LT (8–12 cycles), and again at RT (13–17 cycles) with a current of 0.2 C. Each time on changing the operating temperature, the cells were stored for 4 h prior to the next cycling. All types of the cells were tested by using a multi-channel battery tester (TOYO TOSCAT-3100 U).

Results and discussion

Figure 1 shows the typical charge–discharge curve profiles for the half coin cell. The charge–discharge curves of LL and HL half coin cells that were tested at RT and LT are shown in Fig. 1a, b for the anode and Fig. 1c, d for the cathode. In Fig. 1a, b, graphite electrode with LL and HL showed the 1st discharge capacity around 353 and 357 mAh/g at RT, respectively, but the same cells displayed discharge capacities of 47.88 mAh/g (LL) and 1.40 mAh/g (HL), respectively, when tested at LT. This lowering of the discharge capacity values at LT was due to polarization induced by the internal resistance of the cell. When an anode electrode with HL was discharged at LT, a sudden discharge capacity loss of electrode was observed, which was primarily due to the limited Li ion diffusion into the thicker electrode. When there was a large gradient in the Li-ion concentration for the active material particles

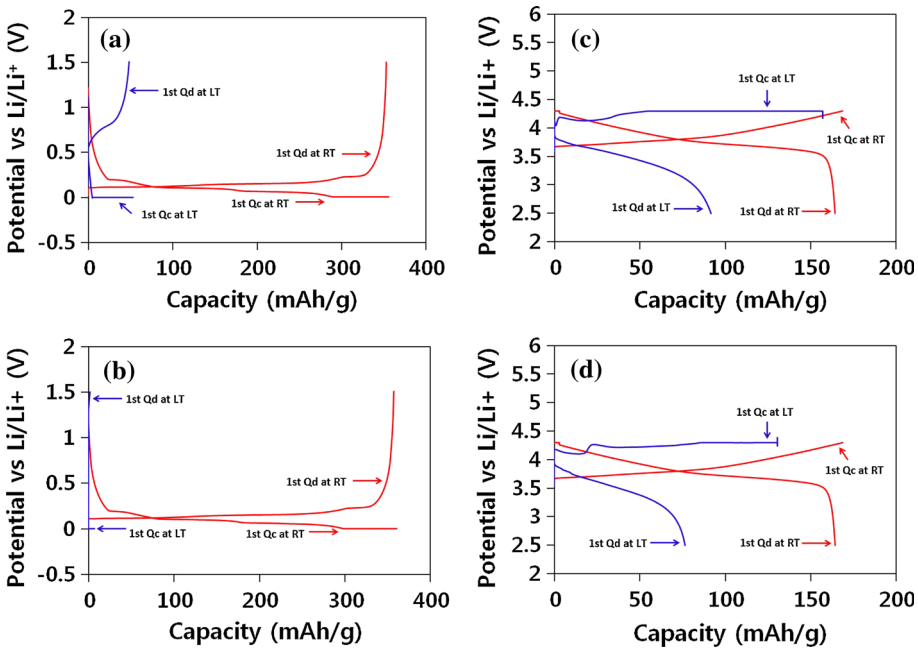

Fig. 1 Typical charge–discharge curves of **a** LL anode, **b** HL anode, **c** LL cathode, and, **d** HL cathode retained at RT and LT

during the discharge, the electrode potential dropped to the cut-off potential. At LT, anode electrodes prepared with LL and HL were able to deliver only 13.56 and 0.392 %, respectively of its RT capacity (capacity retention). For the LL and HL cathode electrodes, a discharge capacity of 165 mAh/g was observed at RT with 0.2 C current density as shown in Fig. 1c, d. The LL and HL cathode electrodes showed the first discharge capacity of 91.78 and 76.29 mAh/g at LT, resulting in a capacity retention of 55.62 and 46.23 %, respectively.

A comprehensive study has been performed to formulate a relation between the loading parameters of the electrode and the electrochemical performance of the cell especially at LT. For this purpose, we extended our study range toward both full coin cell and full pouch cell. Typical capacity profiles (charging capacity, discharging capacity, and Ah efficiency) are shown in Fig. 2a, b for full coin cells prepared with LL and HL. For the full coin cell, the LL anode electrode was paired with the LL cathode electrode and the HL anode electrode was paired with the HL cathode electrode. In case of the full coin cell, the measured first discharge capacities were 1.19 and 3.89 mAh for LL and HL, respectively, at RT at a working current of 0.2 C. The HL full coin cell retained a higher discharge capacity than the LL full coin cell because the thicker electrode with a high loading amount resulted in a higher capacity. At LT, the first discharge capacity of 0.723 and 2.04 mAh for LL and HL full coin cells, respectively, demonstrated the LT behavior. As shown in the Fig. 2a, the full coin cell prepared with a LL showed a stable behavior in terms of charge/discharge capacity and columbic efficiency at LT, while the full coin cell prepared with a HL showed deterioration in capacity and columbic efficiency at LT, as shown in Fig. 2b. Nevertheless, LL and HL full coin cell delivered capacity retention of 60.58 and 52.48 %, respectively. In Fig. 2c, d, LL and HL full pouch cells showed a first discharge capacity of 135 and 401 mAh at RT, 80 and 205 mAh at −32 °C, and delivered capacity retention of 59.25 and 51.12 %, respectively. It can be noted that the full coin cell and the full pouch cell showed a similar retention capacity and columbic efficiency pattern. Moreover, both of these cells with HL showed deterioration in charge/discharge capacity and columbic efficiency at LT. At LT, full-cells (full coin cell and full pouch cell) and cathode half-cells showed better electrochemical performance in terms of better capacity retention, columbic efficiency, and stable cycling behavior than anode half-cells. The full-cells were able to obtain the electric potential difference between the two electrodes through individual measurements at the cathode and anode. On the other hand, the counter electrode of half-cells was used as the reference electrode to facilitate measurements and analysis of activities at the working voltage. The anode half-cells operated at a voltage window was 0.005–1.5 V with charging potential of 0.005 V, which was almost zero. The voltage plateau reached to its limit quickly because of the narrow gap between voltage window, caused by higher ohmic resistance on the surface of anode. This led to capacity fade in anodic half-cells. After LT testing, the full cells were further tested at RT in order to recover from the stress caused by the LT environment. From Fig. 2a–d, it can be noted that the first Ah efficiency value after LT

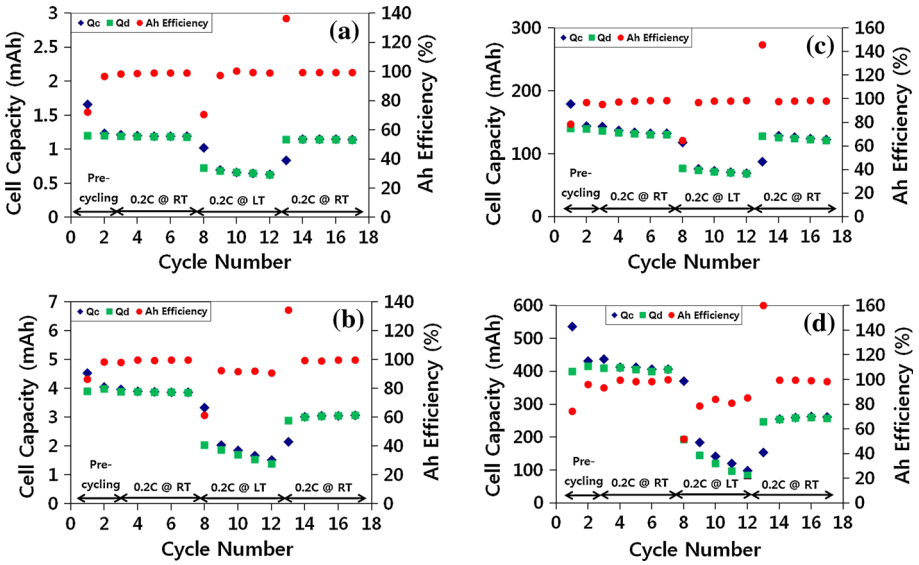

Fig. 2 Typical charge/discharge capacity and Ah efficiency profiles for **a** LL full coin cell, **b** HL full coin cell, **c** LL full pouch cell, and **d** HL full pouch cell retained at RT and LT

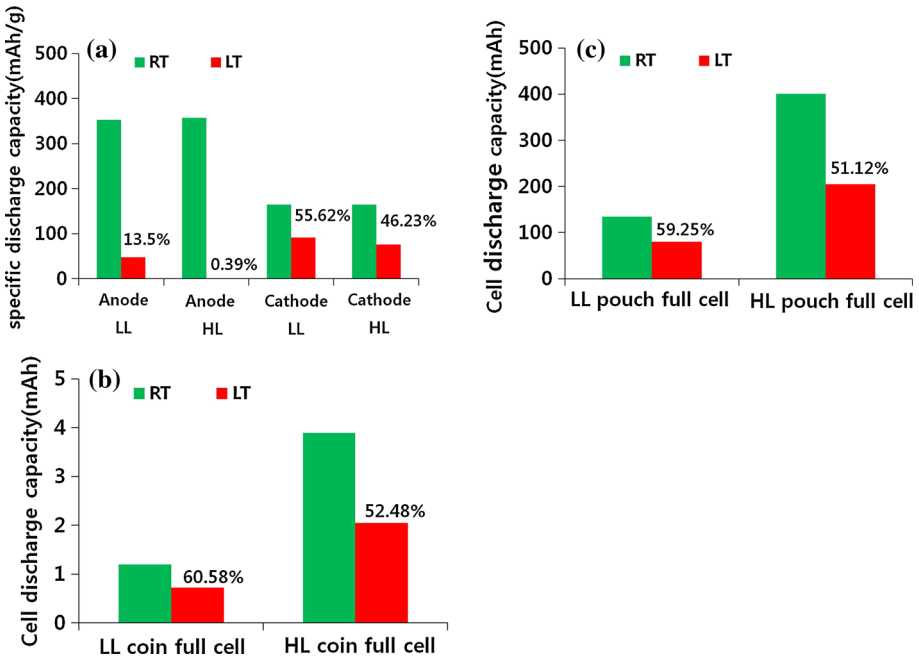

Fig. 3 Graphical profiles of first discharge capacity at LT compared with RT (capacity retention) for **a** half coin cell, **b** full coin cell, and **c** full pouch cell prepared with LL and HL

testing was higher than 100 %. At LT, the charged Li ions were not fully discharged, resulting in a low Ah efficiency. After LT testing, when the cells were cycled at RT, all the Li ions were released, which caused a much higher efficiency. LL full cells (LL full coin cell and LL full pouch cell) showed a stable and consistent behavior with previous RT charge/discharge values, while HL full cells exhibited a drastic decrease because the HL electrode suffered more stress at LT, which caused electrode degradation and capacity fade. From Fig. 2, it is clear that the full coin cell and the full pouch cell shared the same type of chemistry for the cell's electrochemical performance at LT.

The main aim of this work was to compare the retention capacity of all the three cell assembly types with different loadings at LT as shown in Fig. 3. The LL anode, the HL anode, the LL cathode, and the HL cathode showed retention capacity of 13.56, 0.392, 55.62, and 46.23 %, respectively, at LT (Fig. 3a). The LL full coin cell and the full pouch cell showed retention capacities of 60.58 and 59.25 %, respectively, while the HL full coin cell and the full pouch cell showed retention capacities of 52.48 and 51.12 % (Fig. 3b, c). Based on this consistency in the retention capacity values, it can be argued that loading is a primary factor in designing LIBs, especially for a LT

Table 2 First discharge capacity at RT, first discharge capacity at LT, and capacity retention data calculated for half coin cell, full coin cell, and full pouch cell

LD type	Half coin cell						Full coin cell			Full pouch cell		
	Cathode			Anode								
	1st Q_d (RT) (mAh/g)	1st Q_d (LT) (mAh/g)	CR (%)	1st Q_d (RT) (mAh/g)	1st Q_d (LT) (mAh/g)	CR (%)	1st Q_d (RT) (mAh)	1st Q_d (LT) (mAh)	CR (%)	1st Q_d (RT) (mAh)	1st Q_d (LT) (mAh)	CR (%)
LL	165	91.78	55.62	353	47.88	13.56	1.19	0.723	60.58	135	80	59.25
HL	165	76.29	46.23	357	1.40	0.392	3.89	2.04	52.48	401	205	51.12

1st Q_d (*RT*) 1st discharge capacity at 25 °C, *1st* Q_d (*LT*) 1st discharge capacity at −32 °C, *CR* capacity retention (discharge capacity at low temperature compared discharge capacity at room temperature)

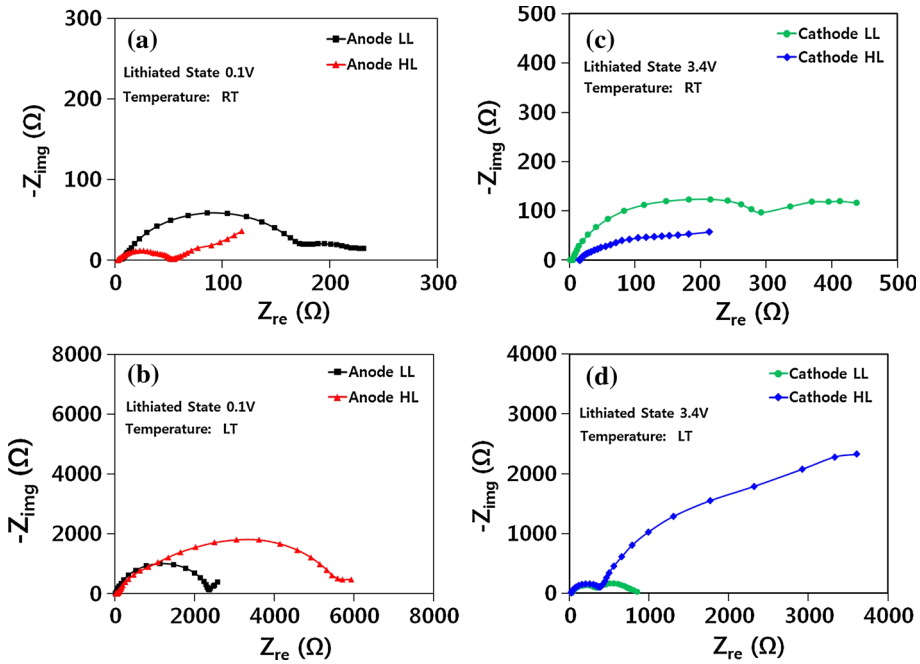

Fig. 4 Nyquist plots of **a** LL and HL anode at RT, **b** LL and HL anode at LT, **c** LL and HL cathode at RT, and **d** LL and HL cathode at LT

environment. The LL full cells showed higher capacity retention and stable cycling behavior at LT because the LL anode contributed electrochemically with the LL cathode, while the HL anode contribution with the HL cathode at LT was minimal. A quantitative analysis of the 1st discharge capacity at RT and LT, and the capacity retentions calculated for the three cell assembly types prepared with LL and HL are presented in Table 2.

Electrode loading can also have an impact on the impedance of a cell. An EIS analysis provided us information on bulk resistance (R_{bulk}) of the electrolyte, separator, and the electrode. The first semi-circle high frequency region represented SEI film resistance (R_{SEI}) of the electrode material. The second semi-circle was the medium frequency range, which indicated the charge-transfer resistance (R_{ct}) of the lithium ions at the electrode interphase [27].

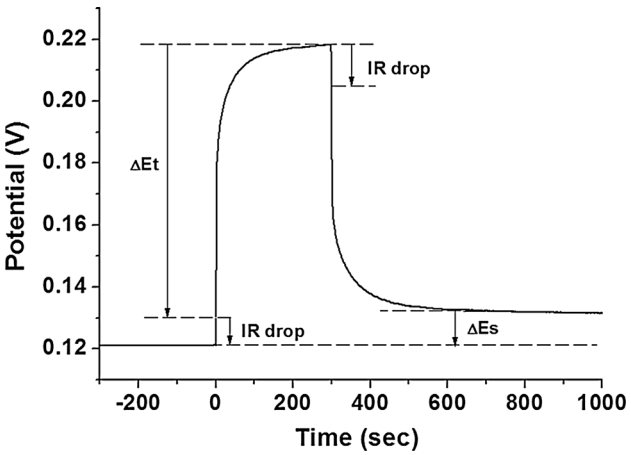

Fig. 5 Typical GITT profile for LL anode with the changes in current and voltage over time at LT during a single-step GITT experiment

Table 3 Lithium diffusion coefficient calculated for LL and HL anode and cathode at RT and LT

Loading type	Cathode		Anode	
	D_{Li+} at RT (cm^2/s)	D_{Li+} at LT (cm^2/s)	D_{Li+} at RT (cm^2/s)	D_{Li+} at LT (cm^2/s)
LL	1.13×10^{-8}	2.46×10^{-10}	1.38×10^{-8}	4.79×10^{-13}
HL	2.78×10^{-8}	1.67×10^{-11}	2.01×10^{-8}	Undefined

D_{Li+} *at RT* lithium diffusion coefficient at 25 °C, D_{Li+} *at LT* lithium diffusion coefficient at −32 °C

The EIS tests were carried out to further understand the reasons for the improved performances of the LL electrodes at LT. The Nyquist plots of the LL anode and the LL cathode at RT were composed by two semicircles at high frequency and a straight small line at low frequency, as shown in Fig. 4a, c. However, the Nyquist plots of the HL anode and the HL cathode electrodes at LT (−32 °C) consisted of one semicircle at high frequency (Fig. 4b, d). At LT, the high-frequency semicircles were hard to notice due to overlapping of the main semicircle, caused by the solid electrolyte interface (SEI). The R_{SEI} was related to the SEI properties formed on the electrode surface. Since SEI properties were not considerably affected by the electrode loading at LT, the magnitude of R_{SEI} for each electrode at different loadings should be relatively stable. R_{ct} represented the resistance of Li ion charge transfer at the electrode/electrolyte interface, which mainly determined the internal cell resistance and was known to be strongly dependent on the electrode potential at a certain temperature. It significantly grew at the end of the discharge when the bulk electrode was about to be saturated with the Li ions [28–30].

Figure 4b, d showed that, the R_{SEI} film resistance, due to overlapping of semicircles was almost negligible for anode and cathode electrodes at LT. Both the HL anode and the cathode showed a higher R_{ct}, than the LL anode and the cathode at LT. This proved that the internal resistance shifted to a higher value when the electrode loading was increased. This was in agreement with the general concept of lowering the electrode resistance through a thinner coating. The rise in the internal resistance was actually the reason for the poor electrochemical performance of the electrode at a higher loading.

Several techniques including EIS and GITT have been used to study the diffusion kinetics of Li^+ intercalation/deintercalation and to estimate the chemical diffusion coefficient of Li^+ (D_{Li+}) in solid electrodes. Similarly, in the current work, an attempt has been made to measure D_{Li+} via GITT. In the GITT method, a constant current was applied during charge/discharge process and the changes in the open-circuit voltage was measured [31, 32]. A constant current helped the lithiation/delithiation process, resulting in concentration gradients at the surface and inner side of the electrodes. The rate of change in concentration was then calculated by measuring the changes in potential over time. From this, D_{Li+} can be calculated.

Figure 5 showed a typical GITT profile for LL anode with certain changes in current and voltage over time at LT during a single-step GITT experiment. The sharp increase or decrease in voltage, when current was applied or cut off, can be explained as a drop in the IR. Any changes in voltage with time were related to the rate of lithium diffusion [33–37]. The diffusion coefficient of lithium can be obtained from GITT using the following equation.

$$D^{\mathrm{GITT}} = \frac{4}{\pi\tau}\left(\frac{m_B V_M}{M_B S}\right)^2 \left(\frac{\Delta E_s}{\Delta E_t}\right)^2.$$

In the above equation, τ was the constant current pulse time (s), m_B was the mass of the insertion electrode material (g), V_M was the molar volume of the electrode material (cm^3/mol), M_B was the molar mass of the insertion electrode material (g/mol), S was the area of the electrode–electrolyte interface (cm^2), ΔE_s was the change in the steady-state voltage during a single-step GITT experiment (V), and ΔE_t was the total change in cell voltage during a constant current pulse τ in a single-step GITT experiment neglecting the IR-drop (V) [38]. D_{Li+} data obtained though single-step GITT experiment at RT and LT are shown in Table 3. D_{Li+} of LL anode at LT was 4.79×10^{-13} cm^2/s, while D_{Li+} for HL anode at LT was out of range, which was in agreement that contribution of the HL anode at LT was minimal. The LL and HL cathode showed 2.46×10^{-10} and 1.67×10^{-11} cm^2/s of D_{Li+}, respectively, which was in agreement that R_{ct} of a thinner electrode, was lower than that of a thicker electrode.

Truly speaking, the capacity loss at LT with increasing electrode loading was not only due to cell polarization but also because of the limited diffusion of the Li ions within the electrode. This clearly proved that the large capacity loss by increasing electrode loading at LT was caused by Li ion diffusion, and was the most important factor influencing the rate performance of the electrode.

Conclusions

Graphite anode and NCM622 cathode with two different loadings were prepared and investigated. Strong impacts of the electrode loading on the capacity retention, columbic efficiency, cycling behavior, cell's internal resistance, and

Li-ion diffusion within electrode matrix, were observed. The deterioration of charge/discharge capacity at low temperature of thicker electrode was mainly due to Li ion diffusion within the electrode and a higher charge-transfer resistance on the surface of electrode. In all the three types of battery assemblies (half coin cell, full coin cell, and full pouch cell), low loaded, thin and low-density electrodes showed a better electrochemical performance, in terms of capacity retention, stable cycling behavior, and Ah efficiency, especially at low temperature. An increase in the internal resistance of the electrode was observed with an increased electrode loading at low temperature. Consequently, a comprehensive understanding and proper optimization of electrode thickness or active material loading is required to design an efficient lithium ion battery for low temperature environment.

Acknowledgements This work was supported by the Next Generation Military Battery Research Center Program of The Defense Acquisition Program Administration and Agency for Defense Development.

References

1. Noel M, Santahnam R (1998) Electrochemistry of graphite intercalation compounds: a review. J Power Sources 72:53
2. Kang K, Meng YS, Breger J (2006) Electrodes with high power and high capacity for rechargeable lithium batteries. Science 311:977–980
3. Farooq U, Yaqub A, Choi JH (2014) Metal-assisted silicon based negative electrode for Li-ion batteries. Mater Lett 126:291–294
4. Pervez SA, Kim DH, Seongju S (2013) Improved performance of Ag-nanoparticles-decorated TiO^2 nanotubes arrays in Li-ion batteries. J Korean Phys Soc 60:1809–1814
5. Pervez SA, Kim DH, Farooq U (2014) Crystalline iron oxide nanotubes arrays with high aspect ratio as binder free anode for Li-ion batteries. Phys Status Solidi A. doi:10.1002/pssa.201330537
6. Tran TD, Feikert JH, Song X (1995) Commercial carbonaceous materials as lithium intercalation anodes. J Electrochem Soc 142:3297–3302
7. Aurbach D, Ein-Eli Y, Chusid O (1994) The correlation between the surface chemistry and the performance of Li-carbon intercalation anodes for rechargeable 'Rocking-Chair' type batteries. J Electrochem Soc 3:603–611
8. Santhanam R, Rambabu B (2009) Improved high rate cycling of Li-rich $Li_{1.10}Ni_{1/3}Co_{1/3}Mn_{1/3}O_2$ cathode for lithium batteries. Int J Electrochem Sci 4:1770–1778
9. Zhang SS, Xu K, Jow TR (2003) The low temperature performance of Li-ion batteries. J Power Sources 115:137–140
10. Park G, Gunawardhana N, Nakamura H (2012) The study of electrochemical properties and lithium deposition of graphite at low temperature. J Power Sources 199:293–299
11. Zhang SS, Xu K, Jow TR (2002) Low temperature performance of graphite electrode in Li-ion cells. Electrochim Acta 48:241–246
12. Zhao G, Wei Z, Zhang N (2012) Enhanced low temperature performances of expanded commercial mesocarbon microbeads (MCMB) as lithium ion battery anodes. Mater Lett 89:243–246
13. Fan J (2003) On the discharge capability and its limiting factors of commercial 18650 Li-ion cell at low temperatures. J Power Sources 117:170–178
14. Ji Y, Zhang Y, Wang CY (2013) Li-ion cell operation at low temperatures. J. Electrochem Soc 160(4):A636–A649
15. Nagasubramanian G (2001) Electrical characteristics of 18650 Li-ion cells at low temperatures. J. Appl Electrochem 31:99–104
16. Patey TJ, Hintennach A, Mantia FL (2009) Electrode engineering of nanoparticles for lithium-ion batteries: role of dispersion technique. J Power Sources 189:590–593
17. Lestriez B, Ligneel E, Guy D (2007) Advanced materials and methods for lithium ion batteries. Transworld Research Network, Kerala, pp 229–256
18. Thorat IV, Stephenson DE, Zacharias NA (2009) Understanding rate-limiting mechanisms in $LiFePO_4$ cathodes for Li-ion batteries. J Power Sources 188:592–600
19. Magasinski A, Dixon P, Hertzberg B (2010) High performance lithium-ion anodes using a hierarchical bottom-up approach. Nat Mater 9(4):353
20. Zhao K, Pharr M, Vlassak JJ (2010) Fracture of electrodes in lithium-ion batteries caused by fast charging. J Appl Phys 108:73517
21. Zheng H, Li J, Song X (2012) A comprehensive understanding of electrode thickness effects on the electrochemical performances of Li-ion battery cathodes. Electrochem Acta 71:258–265
22. Nelson P, Bloom I, Amine K (2002) Design modeling of lithium-ion battery performance. J Power Sources 110:437–444
23. Lu W, Jansen A, Dees D (2011) High-energy electrode investigation for plug-in hybrid electric vehicles. J Power Sources 196:1537–1540
24. Wang M, Li J, He X (2012) The effect of local current density on electrode design for lithium-ion batteries. J Power Sources 207:127–133
25. Doyle M, Fuller TF, Newman J (1993) Modeling of galvanostatic charge and discharge of the lithium/polymer/insertion cell. J Electrochem Soc 140:1526–1533
26. Srinivasan V, Newman J (2004) Design and optimization of a natural graphite/iron phosphate lithium-ion cell. J Electrochem Soc 151:A1530–A1538
27. Yoon S, Hwang IK, Lee CW (2011) Power capability analysis in lithium ion batteries using electrochemical impedance spectroscopy. J Electroanal Chem 655:32–38
28. Tang SB, Lai MO, Lu L (2008) Study on Li^+-ion diffusion in nano-crystalline $LiMn_2O_4$ thin film cathode grown by pulsed laser deposition using CV, EIS and PITT techniques. Mater Chem Phys 111:149–153
29. Momma T, Matsunaga M, Mukoyama D (2012) Ac impedance analysis of lithium ion battery under temperature control. J Power Sources 216:304–307
30. Zhang SS, Xu K, Jow TR (2004) Electrochemical impedance study on the low temperature of Li-ion batteries. Electrochim Acta 49:1057–1061
31. Tang XC, Song XW, Shen PZ (2005) Capacity intermittent titration technique (CITT): a novel technique for determination of Li^+ solid diffusion coefficient of $LiMn_2O_4$. Electrochim Acta 50:5581–5587
32. Pyun SI (2001) Outlines of electrochemistry of materials, Introduction to material electrochemistry. Sigma Press, Rawalpindi
33. Jung KN, Pyun SI (2007) Effect of pore structure on anomalous behaviour of the lithium inter-calation into porous V_2O_5 film electrode using fractal geometry concept. Electrochem Acta 52:55453
34. Jun GH, Hai LX, Ming ZX (2007) Diffusion coefficient of lithium in artificial graphite, mesocarbon microbeads, and disordered carbon. New Carbon Mater 22:7–11

35. Rui XH, Yesiboltati N, Li SR (2011) Determination of the chemical diffusion coefficient of Li^+ in intercalation-type $Li_3V_2(PO4)_3$ anode material. Solid State Ion 187:58–63
36. Shuja KM, Rao GVS, Chowdari BVR (2003) Influence of Li-ion kinetics in the cathodic performance of layered Li $(Ni_{1/3}Co_{1/3}Mn_{1/3})O_2$. J Electrochem Soc 151:A1324–A1332
37. Prosini PP, Lisi M, Zane D (2002) Determination of the chemical diffusion coefficient of lithium in $LiFePO_4$. Solid State Ion 148:45–51
38. Park JK (2010) Principles and applications of lithium secondary batteries. Wiley-VCH, Weinheim, pp 238–239